Dynamic evolution of Rayleigh-Taylor bubbles from sinusoidal, W-shaped, and random perturbations

Zhi-Rui Zhou,[1] You-Sheng Zhang,[1,2,*] and Bao-Lin Tian[1,2,†]

[1]*Institute of Applied Physics and Computational Mathematics, Beijing 100094, China*
[2]*Center for Applied Physics and Technology, Peking University, Beijing 100871, China*

Implicit large eddy simulations of two-dimensional Rayleigh-Taylor instability at different density ratios (i.e., Atwood number $A = 0.05, 0.5,$ and 0.9) are conducted to investigate the late-time dynamics of bubbles. To produce a flow field full of bounded, semibounded, and chaotic bubbles, three problems with distinct perturbations are simulated: (I) periodic sinusoidal perturbation, (II) isolated W-shaped perturbation, and (III) random short-wave perturbations. The evolution of height h, velocity v, and diameter D of the (dominant) bubble with time t are formulated and analyzed. In problem I, during the quasisteady stage, the simulations confirm Goncharov's prediction of the terminal speed $v_\infty = \mathrm{Fr}\sqrt{Ag\lambda/(1+A)}$, where $\mathrm{Fr} = 1/\sqrt{3\pi}$. Moreover, the diameter D at this stage is found to be proportional to the initial perturbation wavelength λ as $D \approx \lambda$. This differed from Daly's simulation result of $D = \lambda(1 + A)/2$. In problem II, a W-shaped perturbation is designed to produce a bubble environment similar to that of chaotic bubbles in problem III. We obtain a similar terminal speed relationship as above, but Fr is replaced by $\mathrm{Fr}_w \approx 0.63$. In problem III, the simulations show that h grows quadratically with the bubble acceleration constant $\alpha \equiv h/(Agt^2) \approx 0.05$, and D expands self-similarly with a steady aspect ratio $\beta \equiv D/h \approx (1 + A)/2$, which differs from existing theories. Therefore, following the mechanism of self-similar growth, we derive a relationship of $\beta = 4\alpha(1 + A)/\mathrm{Fr}_w^2$ to relate the evolution of chaotic bubbles in problem III to that of semibounded bubbles in problem II. The validity of this relationship highlights the fact that the dynamics of chaotic bubbles in problem III are similar to the semibounded isolated bubbles in problem II, but not to that of bounded periodic bubbles in problem I.

I. INTRODUCTION

When a light fluid accelerates a heavy fluid, perturbations at the interface evolve into bubbles (spikes) when the light (heavy) fluid penetrates into the heavy (light) fluid [1]. This process is called Rayleigh-Taylor (RT) instability [2,3] and occurs in systems ranging in scale from microscale [4] (e.g., inertial confinement fusion [5]) to astrophysical [6] (e.g., supernova explosions [7]). The evolution of the process is dependent on the shape of the perturbation [8]. For a periodic single-mode perturbation, isolated bubbles and spikes can be observed [9]. In random multimode perturbations, the instability would rapidly develop into a turbulent mixing regime, comprising spike and bubble mixing zones [1]. Because of mass conservation principles, the evolution of a spike mixing zone can be determined by that of the bubble mixing zone [10–12]. Therefore, it is of fundamental importance to obtain quantitative data on the height and structure of the bubble mixing zone [8,12,13], based on which the bulk of the mixing process can be described. Specifically, the location of bubble fronts, h, and the diameter of the (dominant) bubble, D, are typically used [13–16].

For problems with single-mode perturbations, excluding the possible appearance of the final reacceleration and chaotic stages [9,17], the development of RT instability, beginning from a linear stage with exponential growth, $h(t)$, and then transitioning into a potential stage with quasisteady terminal speed, $v_\infty \approx \mathrm{const}$, has been widely accepted and well formulated [17–24]. Among these theories, Goncharov's potential theory [18] was proved [25] to agree well with the observation [26]. For periodic bubbles forming in either two-dimensional (2D) or three-dimensional (3D) problems, this theory predicts

$$v_\infty = \mathrm{Fr}\sqrt{Ag\lambda/(1+A)}, \qquad (1)$$

where Fr is the Froude number and equals $(3\pi)^{-1/2}$ in the 2D problem, $A \equiv (\rho_h - \rho_l)/(\rho_h + \rho_l) \in [0,1]$ is the Atwood number, g is acceleration, λ is the wavelength of initial perturbation, and ρ_h ρ_l are the densities of the heavy and light fluids, respectively. This theory further predicts that, at the quasisteady stage, the diameter of bubble is approximately equal to the wavelength of the initial perturbation:

$$D/\lambda \approx 1. \qquad (2)$$

In the current 2D problem, this A-independent scaling is qualitatively consistent with the relationship derived by Sohn [19] but conflicts with the earlier numerical implication [27,28] of

$$D/\lambda \approx (1+A)/2. \qquad (3)$$

In experiments [14] and simulations [13,16], D can be measured directly. However, because of Eq. (1), scientists prefer to use λ in their theories [8,15,28]. Therefore, to compare theories

---
*zhang_yousheng@iapcm.ac.cn
†tian_baolin@iapcm.ac.cn

with observations [13,14,16], a relationship between λ and D becomes critical. In 3D problems, a relationship supporting Eq. (2) has been obtained [25]. However, no definite conclusion has been drawn for 2D problems, even though Eq. (3) has been frequently used [13,16,28]. In this paper, single-mode simulations, for different values of A, are first conducted to resolve the discrepancy between Eqs. (2) and (3). As discussed later, our simulations also support Eq. (2) and not the frequently used Eq. (3).

For problems with random multimode perturbations, the associated issue is of greater concern as it is similar to the situations in practical applications. However, the problem is more complex. For the height of the bubble mixing zone, h, based on dimensional analysis [29] and observations [30,31], Youngs et al. suggest the growth law

$$h(t) = \alpha A g t^2, \tag{4}$$

where α is the bubble acceleration constant. This law was subsequently confirmed [26,32] by numerous experiments [14,33] and simulations [4,13,34–37]. As for the diameter of the dominant bubble, D, it is found to expand self-similarly with the height of bubble-mixing zone as

$$D(t) = \beta h(t), \tag{5}$$

where β is the self-similar parameter.

Equations (4) and (5) quantitatively describe the self-similar [37–40] evolution of turbulent RT mixing. To date, it is clear that the self-similar evolution can be achieved through two distinct mechanisms: bubble competition and bubble merger [13,16,26,28,38,41,42]. If the multimode perturbations involve long wavelengths λ that are comparable to the system width L, the late-time mixing would be dominated by the competition between individual long-wavelength bubbles [16,28,43]. In this situation, as the growth of individual waves is closely related to the initial perturbation amplitude and the linear growth rate, the resulting α and β may depend on the initial perturbation amplitude and the material properties [43]. By contrast, if the interface is perturbed entirely by randomly combined waves with individual wavelengths $\lambda \ll L$, the bubbles will expand self-similarly by merging with their smaller neighbors [8,15,29,44–54]. In this situation, the nonlinear coupling of different modes dominates the late-time evolution [42] when the amplitudes of individual waves become comparable to their wavelengths [41], resulting in a universal α and β (i.e., independent of initial perturbation and material properties). As the mechanism of bubble competition is elaborated on in another study [43], in this study, we focus only on the 2D evolution of bubble mergers with random short-wave perturbations.

The description of the bubble merger of a mixing front was pioneered by Sharp and Wheeler (SW) [44], who proposed a 3D model for bubble rising and merging [8]. In their model, given the initial distribution of the radius and height of bubbles, the evolution of the merger process can be simulated by considering the terminal speed of single bubbles, the merger criteria, and the conservation of cross section and volume of the involved bubbles. Following the SW model, Glimm and his coauthors [8,45–49,55] studied a simplified model that considered only the height distribution of the initial bubbles. In this model, based on a delicate choice of the renormalization

scale, a nondimensional differential equation describing the merger process is established [45]. A number of renormalization analyses show that this equation would converge to a fixed point [45], resulting in a universal α and β, in either 2D [45] or 3D [8] problems. However, the model has certain limitations. First, as the correct [18,22,25,26] terminal speed relationship of Eq. (1) had not been established at that time, the A-independent α was obtained using the wrong relationship, $v_\infty = c\sqrt{Ag\lambda}$. Unfortunately, repeating their renormalization process [8,33,45,55] with the correct relationship leads to an A-dependent relation of $\alpha(1 + A) = $ const, in conflict with the observations [14,30,33]. Secondly, this model predicts that β is independent of A, which is inconsistent with the empirical scaling of $\beta = (1 + A)/4$ observed in 3D experiments [14], and $\beta = (1 + A)/2$ observed in our 2D simulations presented in this study.

In contrast to the work of Glimm et al., Alon and his coauthors [15,51–54] proposed a different simplified SW model, in which only the radius distribution of the initial bubbles was considered. In this model, a differential equation describing the merger process is also established [51]. Given the different initial distributions, the analysis shows that the mixing would evolve rapidly into a scale-invariant regime, resulting in a universal $\alpha \approx 0.05$ and $\beta(A) \approx 2(1 + A)$ [15,54]. Although this model successfully captures the variation tendency of α and β with A, the predicted value of β is significantly greater [28] than the observed value in experiments [14] and simulations [13,16]. For example, Dimonte found [14] that the predicted $\beta(A) = 2(1 + A)$ is eight times greater than the experimental value, $\beta(A) = (1 + A)/4$. Oron et al. attributed this difference to dimensionality, and an improved 3D merger model was proposed [54]. However, Dimonte claimed [28] the β predicted by the improved 3D model remained 2–3 times greater than the observed value. In fact, as we will see, even for the 2D problem, the predicted $\beta(A) = 2(1 + A)$ is four times greater than our current simulations.

In summary, neither the Glimm et al. model nor the Alon et al. model can accurately predict both α and β simultaneously, and an improved understanding of the merger process is required. After a thorough investigation of the above two models, we find that, in essence, both models depend on two common factors: (1) the nondimensional coefficient of the terminal speed Fr and (2) the two-bubble merger rate, ω. ω is defined as the inverse of the time interval between the time at which the two bubbles have the same speed and the time at which the movement of the smaller bubble stops [29,45,52,53,55,56]. Consequently, for chaotic RT mixing, an accurate prediction of α and β can be achieved, provided that the actual values of Fr and ω are used. As we know, however, the values of Fr and ω are highly dependent on the shape and environment of the bubble [28,50,57–59]. In the Alon et al. model, both Fr and ω are determined by the periodic arising bubbles. However, this bounded environment obviously differs from the real environment of chaotic RT bubbles, and we propose that this is the reason for the failure of their model. In fact, the bubbles of chaotic RT mixing lie in a semibounded environment [28], with a larger Fr. By merely observing this difference [29], Glimm et al. proposed the assumption of superposition to increase the single bubble velocity by adding the velocity of modulated envelope [8]. However, as discussed

by Dimonte [28], this may not be required, as any bubble that is perturbed forward will behave more like an isolated or semibounded bubble. Therefore, we need to produce only an environment similar to that of chaotic RT bubbles and measure the corresponding Fr. In accordance with this theory, in this study, a W-shaped perturbation is imposed to simulate the chaotic environment and to connect the evolution of chaotic RT mixing with that of semibounded bubbles.

This study investigates the dynamic characteristics of 2D RT bubbles evolving from different types of perturbations with different density ratios. In Sec. II, we describe the numerical framework and problem setup. In Sec. III periodic sinusoidal perturbations, isolated W-shaped perturbations, and random short-wave perturbations are designed to investigate the late-time evolution of 2D RT bubbles in bounded, semibounded, and chaotic environments. The corresponding results and discussions, as well as a theoretical relationship to explain the difference between previous theories and simulations, are discussed in this section. The conclusions are presented In Sec. IV.

II. COMPUTATIONAL FRAMEWORK

A. Numeric

Direct numerical simulation (DNS) is the most widely accepted method to accurately simulate a flow [60]. In DNS, the grid number is proportional to $Re^{9/4}$, where Re is the Reynolds number. For current RT problems of interest (e.g., inertial confinement fusion and supernova explosions), the Re involved is typically extremely large. Consequently, the corresponding computing requirements cannot be met. Fortunately, for RT mixing with high Re, Youngs [32] has shown that implicit large eddy simulations (ILESs) can yield results comparable to that of DNS, at least for large-scale dynamic quantities such as α and β, that are currently of interest [32]. Therefore, an ILES is used in this study. The following compressible Eulerian equation (6) and mass fraction equation (7) are solved:

$$\begin{cases} \frac{\partial}{\partial t}(\rho) + \frac{\partial}{\partial x_j}(\rho u_j) = 0 \\ \frac{\partial}{\partial t}(\rho u_j) + \frac{\partial}{\partial x_j}(\rho u_i u_j + p\delta_{i,j}) = -\rho g, \\ \frac{\partial}{\partial t}(\rho e) + \frac{\partial}{\partial x_j}[(\rho e + p)u_j] = -\rho u_i g \end{cases} \quad (6)$$

$$\frac{\partial}{\partial t}(\rho Y) + \frac{\partial}{\partial x_j}(\rho u_j Y) = 0, \quad (7)$$

where $x_{i=1,2}(x \equiv x_1, y \equiv x_2)$ is the space direction, and ρ, u, p, e, Y, and g are density, velocity, pressure, total energy per unit mass, mass fraction, and acceleration, respectively. The acceleration g is in the y direction. Equations (6) and (7) are solved with the equation of state for an ideal gas

$$\rho e = p/(\gamma - 1), \quad (8)$$

where γ is the specific heat ratio. The thermodynamic quantities of mixed materials are modeled with the following isothermal and partial pressure assumptions [61]:

$$\begin{cases} f = f_1 + f_2; f = \rho, p \\ f = f_1 = f_2; f = T, V \\ f = Y f_1 + (1 - Y)f_2; f = C_p, C_v \end{cases} \quad (9)$$

Specifically, the density and pressure of the mixture are obtained by the addition of the corresponding physical variables of each fluid. The volume and temperature of the mixture are equal to that of each fluid, while the physical property parameters, such as specific heat at constant volume, are obtained by a linear combination with the mass fractions.

To simplify the simulation, we use an ideal gas for both the heavy and light fluids. Considering this configuration, Eq. (7) is introduced primarily for visualizing and tracing the interface between two fluids. Moreover, we emphasize that the volume fraction of the heavy fluid, $\varphi \equiv \rho Y/\rho_h$, is introduced for visualization as it is more accurate in tracing the interface under large density ratio situations [13]. The entire simulation is implemented in our developed compressible Eulerian program, known as the Code of Finite Difference for Compressible Fluid Dynamics (CFD²). The movement over time adopts a third-order accurate total variation diminishing Runge-Kutta scheme, with CFL = 0.5. The convection term is solved with an HLL Riemann solver and a seventh-order WENO scheme [62].

B. Initialization

Similar to the initialization adopted by the Alpha Groups [13], in this simulation, we use the compressible configuration to approach a quasi-incompressible regime. Specifically, for an initial resting flow field (i.e., $u_i = 0$), the profiles of density and pressure are derived by first satisfying the hydrostatic equilibrium

$$\partial p/\partial y = -\rho g. \quad (10)$$

Furthermore, to maintain the effective Atwood number (Atwood number in mixing region) approximately constant, Eq. (10) is solved with the adiabatic relationship

$$p/\rho^\gamma = \text{const} \quad (11)$$

to give [13]

$$\rho(y) = \rho_0 \left(1 - \frac{\gamma - 1}{\gamma} \frac{\rho_0 g y}{p_0}\right)^{\frac{1}{\gamma - 1}}. \quad (12)$$

The corresponding pressure profile, $p(y)$, can be obtained by combining Eq. (11) with Eq. (12). In Eq. (12) $\rho_0 = \rho_h$ for $y \geqslant 0$, and $\rho_0 = \rho_l$ for $y < 0$, γ is set as 5/3 for both fluids, and $g = 2 \text{ cm/s}^2$ is in the y direction. Here p_0 is an important quantity, as a larger p_0 makes the simulation more incompressible. However, it also shortens the time step so that more computing resources are required. From previous studies, p_0 needs to be sufficiently large to limit the vertical density variation to below 6%. It is typically acceptable to set $p_0 = 2\pi(\rho_h + \rho l)gL$; however, in large density ratio simulations, a larger p_0 is needed.

As for perturbations, with the aid of linear theory, the imposed perturbations at the interface are converted to a velocity field (see more details in Ref. [13]). We impose the velocity perturbations only on the interface ($y = 0$). To produce a flow field full of bounded, semibounded, and chaotic bubbles, three distinct perturbations are imposed, as shown in Fig. 1. These are the periodic sinusoidal perturbation, the isolated W-shaped perturbation, and random short-wave
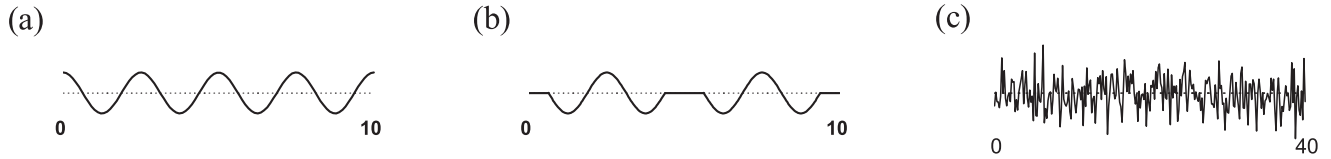
FIG. 1. Velocity on interface ($y = 0$) of (a) periodic sinusoidal perturbation, (b) W-shaped perturbation, and (c) random short-wave perturbations.

perturbations. The amplitudes in Fig. 1 indicate the values of the initial velocity on the interface.

The shape of periodic sinusoidal perturbation is given by the relationship

$$\dot{h}(x,0) = 0.01 \cos\left(\frac{2\pi}{\lambda}x\right), \tag{13}$$

with the perturbation wavelength $\lambda = 2.5$ cm. The W-shaped perturbation has a similar relationship:

$$\dot{h}(x,0) = \begin{cases} 0.01 \cos\left(\frac{2\pi}{\lambda}x\right) & 0.625 \leqslant x \leqslant 4.375 \\ & \text{and } 5.625 \leqslant x \leqslant 9.375 \\ 0 & \text{else.} \end{cases} \tag{14}$$

Bubbles rising from the W-shaped perturbation evolve in a semibounded environment, and their degree of freedom can be estimated by the length of the gap between them. In this way, we can simulate and study an environment that is similar to that in multimode flows. In addition, two troughs on either side of the crest are specifically designed to ensure that the bubbles grow symmetrically. The random short-wave perturbations are set as

$$\dot{h}(x,0) = \sum_k \Gamma(k)c(k)\cos(kx), \tag{15}$$

where we choose 1000 high-k modes waves randomly between modes 16 and 32, $\Gamma(k) \equiv \sqrt{Agk}$ is the exponential growth rate, and $c(k)$ is randomly chosen with a root mean square amplitude $\bar{c} \sim 10^{-3}$. In random short-wave simulations, the horizontal length is enlarged four times to introduce more bubbles into the computation field. This enhances the accuracy when calculating the average bubble diameters.

Finally, in single-mode simulations, we use 32 grids for one wavelength ($\lambda/\Delta = 32$), despite the Alpha Group [13] suggesting that 8 grids ($\lambda/\Delta = 8$) are sufficient. In multimode

flows, we apply a grid resolution (512 grids for 40 cm) similar to the Alpha Group's [13]) settings (128 grids for 10 cm).

C. Cases and definitions

To cover the RT evolution from different perturbations, nine cases (at three representative values of A) were designed and are presented in Table I. In all nine simulations, h is defined as the distance between the interface and the cross section where the x direction averaged-volume fraction of the heavy fluid is 0.99. As for D, since the bubbles in simulations 1–6 have regular shapes, we can readily obtain $D(t)$ by determining the width of the broadest bubble cross section. In simulations 7–9, we use an autocorrelation-based technique [13,16]) to determine the averaged bubble diameters. As no long-wave perturbations are introduced in the initial perturbations, a pure bubble merger mechanism dominates the evolution. The simulation results are presented and discussed in Sec. III.

III. SIMULATION RESULTS

A. Periodic sinusoidal perturbation

In this subsection, we use single-mode simulations (simulations 1–3) to study the evolution of bubble velocity, $v(t)$, and bubble diameter, $D(t)$. The velocity evolution is used to infer the nondimensional velocity coefficient Fr, defined as $\text{Fr}(t) \equiv v(t)/\sqrt{Ag\lambda/(1+A)}$. At the terminal speed stage, the good agreement in Fr between the current simulations and Goncharov's theory [18] validates our code, and D is measured to establish a quantitative relationship with initial perturbation wavelength, λ, and A. Based on this, the established theoretical relationship can be transferred between λ and D (see details in Sec. III C).

TABLE I. List of simulations.

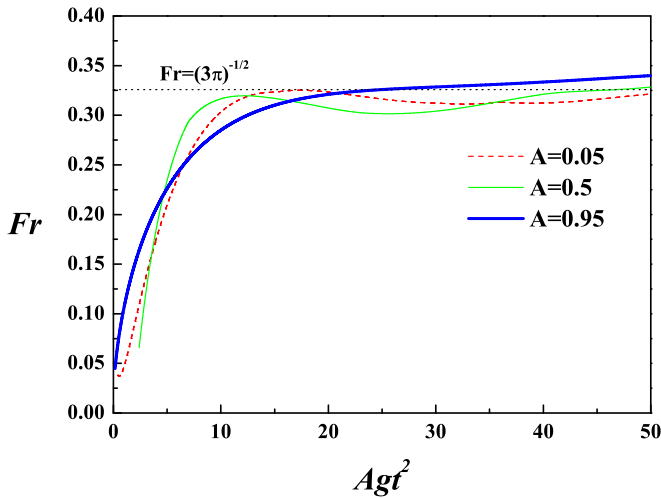| Simulation no.	Perturbation type	Atwood number	Domain size (cm)	Mesh size
1		0.05		
2	Periodic sinusoidal	0.5		
3		0.95		
			$[0,10] \times [-10,10]$	128×256
4		0.05		
5	W-shape	0.5		
6		0.95		
7		0.05		
8	Random short-wave	0.5	$[0,40] \times [-10,10]$	512×256
9		0.95		

FIG. 2. Evolution of Fr at three representative density ratios in bounded environment.

1. Evolution of Fr

As discussed in the introduction, before the possible appearance of the final reacceleration and chaotic stages [9], the development of single-mode RT bubbles starting from a linear stage, and then transitioning into a potential stage, has been widely recognized. Researchers have conducted numerous investigations to find analytical laws valid from the linear stage to the potential stage. In the potential stage, various numerical simulations and theories [18,22] have indicated that bubbles will attain a quasisteady terminal velocity, satisfying Eq. (1), with the widely accepted constant $Fr \approx (3\pi)^{-1/2}$ in the 2D problem. Figure 2 shows the evolution of $Fr(t)$ for simulations 1–3. First, Fr increases rapidly, and then stabilizes at approximately $Agt^2 = 10$ cm. Finally, Fr reaches a quasisteady value (corresponding to terminal velocity). From this figure, we can see that, for all three typical density ratios,

the final quasisteady values correlates well with the theoretical values, $(3\pi)^{-1/2}$. The agreement validates our simulations.

2. Relationship between D and λ

As shown in Eq. (1), in theoretical studies [8,15,28], researchers prefer to express the quasisteady terminal speed, v_∞, with the perturbation wavelength λ, as λ is closely coupled to the initial conditions and remains constant during single-mode RT evolutions. However, in experiments [14] and simulations [16,28], researchers favor the use of D, as it can be directly measured. Therefore, before the establishment of a unified formula between the terminal speed (v_∞) and the characteristic length (λ and D), it is meaningful to obtain a relationship between D and λ. However, for the 2D problem, a definite relationship has not yet been established.

In 3D problems, the relationship of Eq. (2) is accepted by researchers. By contrast, there are still ambiguities in 2D situations. Earlier 2D simulations by Daly [27] first implied the relationship of Eq. (3) [28]. The rationality of Eq. (3) has been discussed by Dimonte [28], who considered, at $A = 1$, that $D = \lambda$ is reasonable as the spikes are extremely narrow. By contrast, at $A = 0$, the relationship should be $2D = \lambda$, as the spikes are identical to the bubbles. After rechecking the original data, however, we find that Daly ended his simulations before the bubbles approached the steady potential stage, especially for the simulations with lower A. This conclusion can be obtained from the following considerations. The widely validated relationship of Eq. (1) implies that Fr is an A-independent constant. However, recalculating Fr with the data given in the literature [27] shows that Fr is less than the theoretical value of $(3\pi)^{-1/2}$, especially for the simulations with lower values of A. Consequently, the correctness of Eq. (3) becomes questionable. In fact, in contrast to Daly's relationship, Alon et al. [15] asserted an A-independent relationship of Eq. (2), based on a buoyancy-drag model. In their later works [54,63], this relationship was also adopted when analyzing data. Finally,
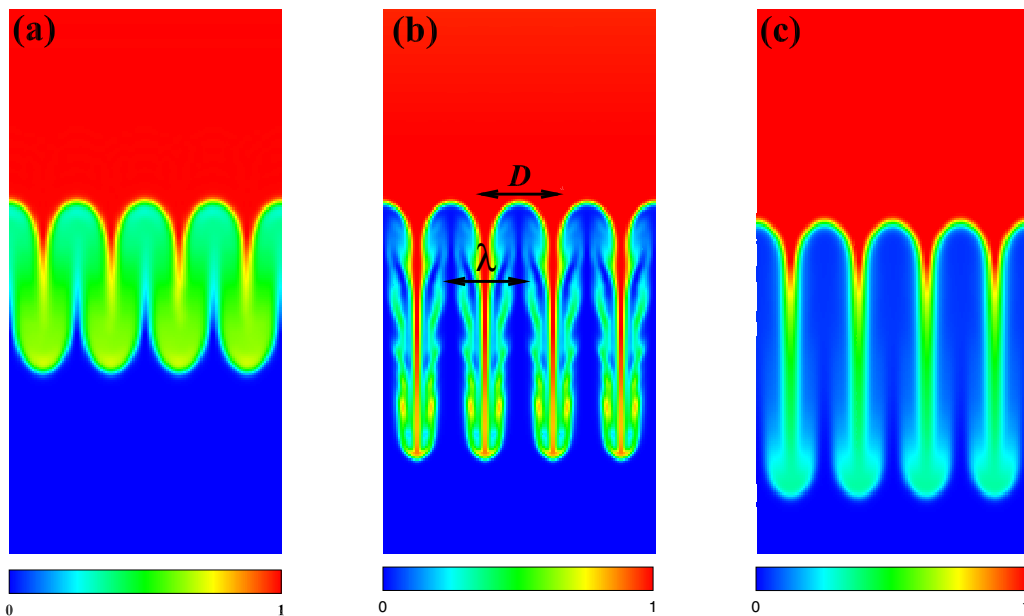

FIG. 3. Volume fraction distributions for late-time single-mode evolution at (a) $A = 0.05$, (b) $A = 0.5$, and (c) $A = 0.95$.
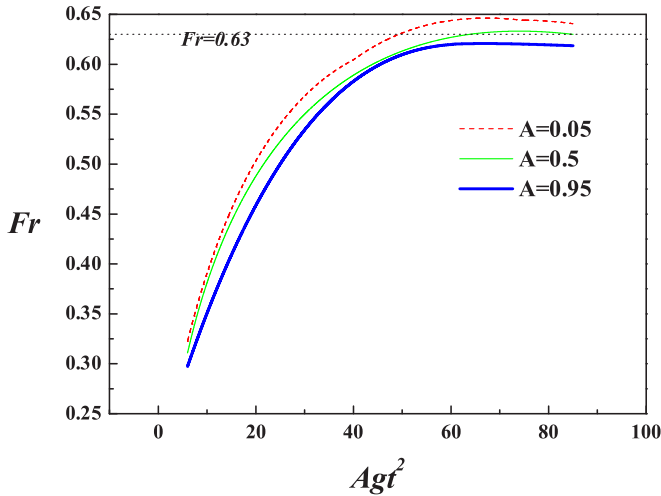
FIG. 4. Evolution of Fr at three typical density ratios in semi-bounded environment.

from Goncharov's and Sohn's theory [18,19], a relationship similar to Eq. (2) can also be derived, to give $D/\lambda \approx$ const.

In this study, single-mode simulations at different values of A are conducted to clarify this relationship. In Fig. 3 we plot the contours of volume fractions from simulations 1–3 when the bubbles reach their terminal velocities. As can be seen, there is no gap between bubbles in all three simulations. From these, we find $D = 2.5$ cm, which is approximately equal to the perturbation wavelength λ, supporting the relationship of Eq. (2).

As opposed to Dimonte's explanation for Eq. (3), we explain the rationality of Eq. (2) with the drag-buoyancy model [64], as follows. A given isolated RT bubble is subjected to three forces: buoyancy force, drag force, and inertial force. As larger bubbles have less drag but equal buoyancy per unit mass, RT bubbles tend to grow larger. Consequently, lower drag leads to higher speeds, and this reinforces this cycle. Therefore, the bubbles will not stop expanding until the gaps between them are covered. In other words, the bubbles will not attain a steady terminal speed until they have fully expanded. In the following sections, the relationship of Eq. (2) is adopted, and only D is used as the characteristic bubble width, to avoid ambiguity.

B. W-shaped perturbation

In this subsection, a W-shaped perturbation is designed to study the evolution of the Fr number when RT bubbles develop in a semibounded environment. Semibounded environments fall between the periodic bounded environment shown above and the unbounded environment where bubbles develop totally free from their neighbors. As discussed in the introduction, in this study we propose that multimode RT bubbles develop in an environment similar to the semibounded environment. As shown in Fig. 5(b), for the late-time evolution of chaotic RT bubbles, there are obvious gaps between adjacent multimode RT (dominant) bubbles, and the average length of the gaps is typically comparable to the average bubble diameter. As the value of Fr is closely coupled to the environment and the shape of bubbles [28], we investigate the evolution of Fr in problems with W-shaped perturbations, aiming to indirectly determine Fr in multimode flows.

In earlier work, Collins [65] designed a plane experiment to simulate 2D bubble evolution in infinite space and determined Fr ≈ 0.5. However, the bubble in Collins's experiment comprised only the bubble cap, while a regular RT bubble [as shown in Fig. 5(a)] comprises a bubble cap and a bubble stalk. As discussed above, the value of Fr for a bubble depends on its environment and shape. Physically, the bubble cap is subjected to significantly more drag per mass than the bubble stalk. Therefore, the Fr number of a bubble cap may be less than that of a complete bubble.

Similarly, in a semibounded environment, the evolution of $\mathrm{Fr}(t) \equiv v(t)/\sqrt{AgD(t)/(1+A)}$ can be obtained with simulations. Figure 4 shows the results from simulations 4–6. The figure shows that, regardless of the initial period, the value of Fr stabilizes at approximately $\mathrm{Fr}_w \approx 0.63$. The dependence of Fr on the density ratio is weak. Figure 5 shows the environment of W-shaped flow and multimode flow at a typical time. The average length of the gaps between the dominant bubbles in Fig. 5(b) is comparable to the average diameter of the dominant bubbles and is similar to that shown in Fig. 5(a). Based on this similarity, as described in the next section, we use the obtained $\mathrm{Fr}_w = 0.63$ to establish a theoretical relationship between multimode flows and semibounded flows.

Following the logic in Sec. III A and Sec. III B, we discuss two cases. Case I: If one waits long enough, two neighboring
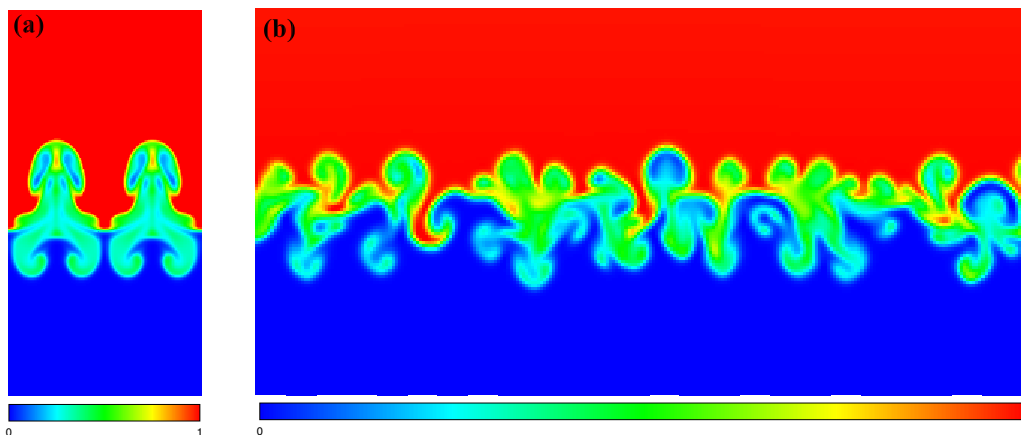

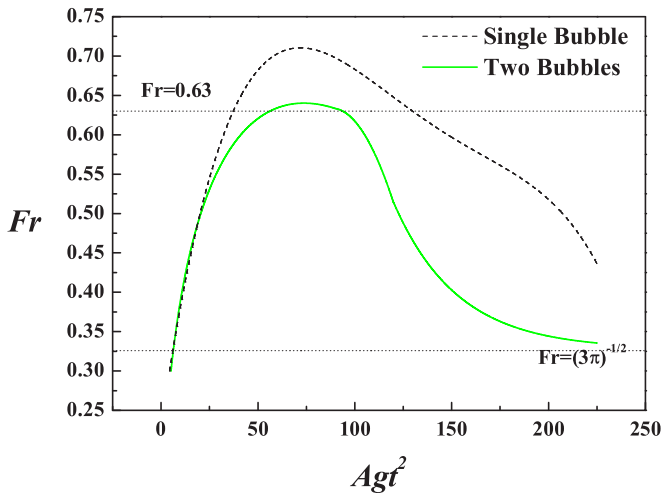FIG. 5. Late-time environment ($A = 0.5$, time $= 8$ s) for (a) semibounded flow and (b) multimode flow.

FIG. 6. Evolution of Fr in case I (green solid line) and case II (black dashed line).

semibounded bubbles will get close and become bounded bubbles, so the value of Fr may go down and reach $(3\pi)^{-1/2}$. Case II: If there exists an unbounded bubble, the bubble will continue expanding and the Fr will get even larger than 0.63. We implement simulation 5 to study case I. In order to avoid the influence of the y-direction boundary, the computational length in the y direction is enlarged twice. As for case II, we modify the simulation in case I by only putting one W-shaped perturbation in the middle of the domain.

The green solid line in Fig. 6 shows the evolution of Fr in case I. After the semibounded stage, the value of Fr goes down and finally stabilizes near $(3\pi)^{-1/2}$. Figures 7(Ia)–7(Ie) shows the evolution of the two bubbles. At late time, they gradually get close and almost become bounded bubbles. The black dashed line in Fig. 6 shows the Fr evolution of an unbounded bubble. In the beginning, since the bubbles grow in a similar environment, the Fr evolution is almost the same as that in case I. Because there is no bound, the value of Fr continues growing even after reaching 0.63. Later, the bubble keeps expanding both vertically and horizontally at a high speed, and, meanwhile, the spikes keep pressing the root of the bubble. These two factors result in the thinning of bubble stalk, which finally leads to the complete escape of bubble [see in Figs. 7(IIa)–7(IIe)]. During this period, the value of Fr goes down, due to the same reason as Collins's isolated bubble. However, since this simulation does not involve surface tension, the late-time bubble cannot maintain its shape and will continue expanding horizontally. In this case, the value of Fr keeps going down rather than stabilizing at 0.5 as Collins claimed. As this paper mainly studies bubbles which have similar shapes as late-time multimode bubbles [such as the bubbles in Fig. 5(b)], we focus on only the early evolution of the unbounded bubble and do not further discuss its late-time expansion. From the results above, the logic in Sec. III A and Sec. III B is validated.

C. Random short-wave perturbations

Multimode flows are currently of interest, as RT perturbations, with numerous short wavelengths are considered to be
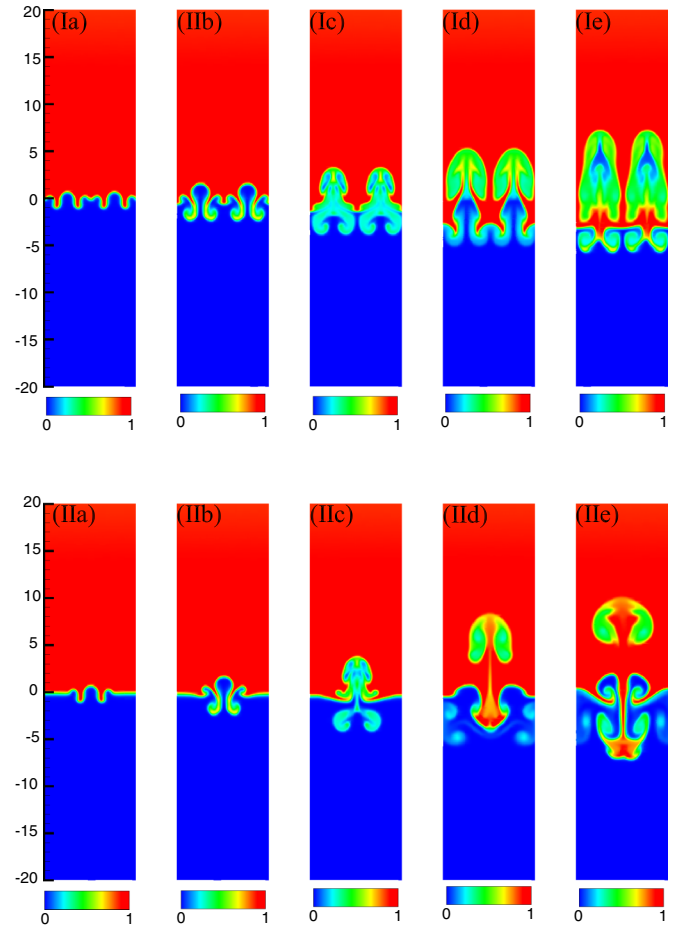

FIG. 7. Volume fraction distributions for bubble evolution at (a) 4 s, (b) 6 s, (c) 8 s, (d) 12 s, and (e) 15 s.

more relevant for practical applications. The greatest problem in practical applications is the growth and structure of the mixing zone. The bubble acceleration constant, α, can predict the growth of the mixing zone, while the self-similar parameter, β, is useful in describing the structure of bubbles. Simulations 7–9 are designed to study the evolution of α and β. In this subsection, we explain theoretically the numerical results and discuss the inconsistencies between current simulations and the prediction of Alon's merger model.

Figure 8(a) shows the variation of bubble height, h, from simulations 7–9. According to Eq. (4), the gradient indicates the value of α. In all three simulations, the gradients vary marginally around 0.05. Figure 8(b) shows the variation of A-renormalized self-similar geometry parameter $\beta/(1 + A)$. It can be seen from this figure that, at late time, β remains steady at $(1 + A)/2$, and the average shape of dominant bubbles remains constant. The calculated α is consistent with the Alon *et al.* merger model prediction, but β is four times smaller than the prediction. Based on the results obtained in Sec. III B, this inconsistency is explained below.

As discussed in the introduction, Alon's merger model is a simplified SW model. This model suggests that multimode RT bubbles evolve through merging smaller bubbles. Under this hypothesis, the flow eventually evolves into a scale-invariant regime, where the initial conditions will be forgotten.
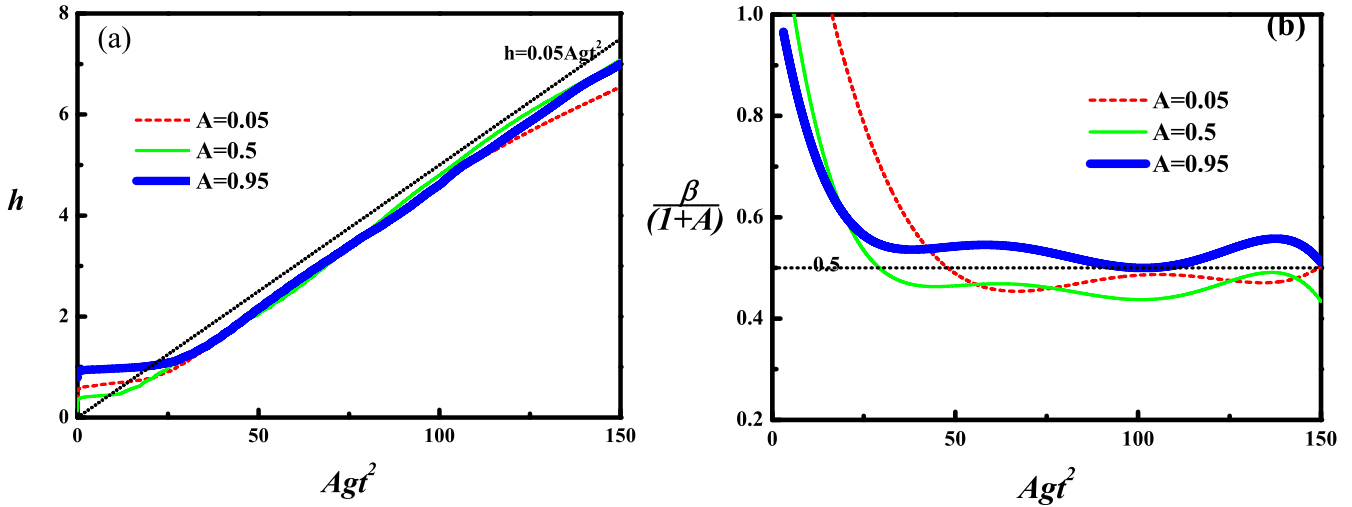
FIG. 8. Evolution of (a) bubble height and (b) self-similar rate (scaled with $(1 + A)$) in multimode flows.

Based on the scale-invariant regime, Alon derived a constant acceleration, $\alpha = 0.051$ [52]. By working with the concept of bubble merger [28], we can derive a relationship of β by combining Eqs. (1), (2), (4), and (5) as [16]

$$\beta = \frac{4\alpha(1 + A)}{Fr^2}. \tag{16}$$

As can be seen, we can obtain $\beta \approx 2(1 + A)$ by introducing $\alpha = 0.05$ and $Fr = 1/\sqrt{3\pi}$ into Eq. (16). Although $\alpha = 0.051$ is an accepted value, $\beta \approx 2(1 + A)$ is not valid. Oron's 2D simulation results also disagreed with this conclusion. Specifically, Oron's simulation obtained $\beta = 2$ at $A = 0.5$, when $\beta = 3$ should have been the result according to their merger model.

In fact, in the Alon *et al.* model, they assumed that the bubble-merging environment at late time is similar to that of periodically arising bubbles in a bounded environment. Therefore, their conclusion is established based on the Fr of periodically arising bubbles. However, as can be seen in Figs. 9(b) and 9(c), late-time bubbles are not always bounded together, and, typically, the bubbles grow freely without competing with their neighbors. When a generation of bubble merger ends, gaps are generated between new merged bubbles. The new bubbles then continue to expand freely until they touch their neighbors, and the next merger generation begins. At late time in multimode RT evolution, as the bubbles are usually large, the interval between generations can be long. In this case, we argue that the bubbles grow in an environment similar to the semibounded environment. Thus, introducing $Fr = 0.63$ into

Eq. (16), we obtain $\beta = (1 + A)/2$, which correlates well with our numerical results.

IV. CONCLUSIONS

The primary aim of this study was to quantitatively investigate the late-time merger evolution of 2D chaotic RT bubbles, with the aid of the two most important physical quantities (α and β) to characterize the bulk of the dynamic process. To this end, simulations with periodic sinusoidal perturbations and W-shaped perturbations were carried out, first, to establish some basic relationships and determine some critical parameters, followed by simulations with random short-wavelength perturbations. The simulations were conducted at three typical values of A (0.05, 0.5, and 0.95) to consider the possible effects of density ratio.

Our single-mode perturbation simulations not only confirmed Goncharov's predictions of Eqs. (1) and (2), but also invalidated the frequently used relationship of Eq. (3) for the first time. The W-shaped perturbation was designed specifically to test our hypothesis: the dynamics of chaotic bubbles are similar to the semibounded isolated bubbles with W-shaped perturbations, but not to bounded bubbles with periodic sinusoidal perturbations. The simulations produced a similar terminal speed relationship as for single-mode sinusoidal perturbations, but the nondimensional velocity coefficient, Fr, approximately doubled to $Fr_w \approx 0.63$. Our multimode evolution simulations suggested $\alpha \approx 0.05$ and $\beta = (1 + A)/2$. Although a similar bubble acceleration constant α was obtained, the self-similar
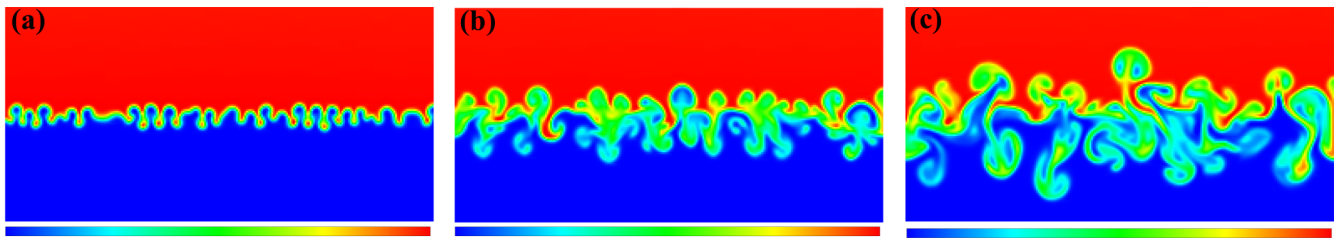

FIG. 9. Multimode evolution with $A = 0.5$ at (a) time = 5 s, (b) time = 8 s, and (c) time = 11 s.

rate in our results was four times smaller than the Alon *et al.* prediction. To explain this difference, a theoretical relationship [Eq. (16)] was established by following the concept of a bubble merger model. From this relationship, we verified that this difference is essentially attributed to the doubling of Fr. The success of relating α to β with Fr$_w$ indirectly validates our hypothesis. This success further implies that (1) qualitatively, the mechanism of bubble merger is correct, and (2) quantitatively, the merger process can be accurately predicted only if reasonable physical parameters are used.

Therefore, the entire merger model depends on two critical parameters: Fr and ω. As discussed in the introduction, however, the values of both parameters are closely coupled to the environment and shape of RT bubbles. The success of Fr$_w$, while not the classical Fr $= (3\pi)^{-1/2}$, in relating α to β implies that the actual evolution of chaotic RT bubbles cannot be characterized with parameters determined from periodic bounded bubbles, as adopted in previous studies. Based on this, an improved bubble merger theory that can correctly predict both α and β simultaneously with physical Fr and ω is expected. However, this is beyond the scope of this study and will be published elsewhere.

[1] B. L. Cheng, J. Glimm, and D. H. Sharp, Phys. Rev. E **66**, 036312 (2002).

[2] L. Rayleigh, Proc. London Math. Soc. **14**, 170 (1883).

[3] G. Taylor, Philos. Trans. R. Soc. A **201**, 192 (1950).

[4] K. Kadau, C. Rosenblatt, J. L. Barber, T. C. Germann, Z. Huang, P. Carles, and B. J. Alder, Proc. Natl. Acad. Sci. USA **104**, 7741 (2007).

[5] R. D. Petrasso, Nature (London) **367**, 217 (1994).

[6] D. Livescu, Philos. Trans. R. Soc. A **371**, 20120185 (2013).

[7] A. Burrows, Nature (London) **403**, 727 (2000).

[8] B. L. Cheng, J. Glimm, and D. H. Sharp, Chaos **12**, 267 (2002).

[9] T. Wei and D. Livescu, Phys. Rev. E **86**, 046405 (2012).

[10] B. L. Cheng, J. Glimm, and D. H. Sharp, Phys. Lett. A **268**, 366 (2000).

[11] B. L. Cheng, J. Glimm, D. Saltz, and D. H. Sharp, Physica D **133**, 84 (1999).

[12] Y. S. Zhang, Z. W. He, F. J. Gao, X. L. Li, and B. L. Tian, Phys. Rev. E **93**, 063102 (2016).

[13] G. Dimonte, D. L. Youngs, A. Dimits, S. Weber, M. Marinak, S. Wunsch, C. Garasi, A. Robinson, M. J. Andrews, P. Ramaprabhu *et al.*, Phys. Fluids **16**, 1668 (2004).

[14] G. Dimonte and M. Schneider, Phys. Fluids **12**, 304 (2000).

[15] U. Alon, J. Hecht, D. Ofer, and D. Shvarts, Phys. Rev. Lett. **74**, 534 (1995).

[16] P. Ramaprabhu, G. Dimonte, and M. J. Andrews, J. Fluid Mech. **536**, 285 (2005).

[17] P. Ramaprabhu, G. Dimonte, P. Woodward, C. Fryer, G. Rockefeller, K. Muthuraman, P. H. Lin, and J. Jayaraj, Phys. Fluids **24**, 074107 (2012).

[18] V. N. Goncharov, Phys. Rev. Lett. **88**, 134502 (2002).

[19] S.-l. Sohn, Phys. Rev. E **67**, 026301 (2003).

[20] S. I. Abarzhi, J. Glimm, and A. D. Lin, Phys. Fluids **15**, 2190 (2003).

[21] Q. Zhang, Phys. Rev. Lett. **81**, 3391 (1998).

[22] Q. Zhang and W. X. Guo, J. Fluid Mech. **786**, 47 (2016).

[23] K. O. Mikaelian, Phys. Rev. E **67**, 026319 (2003).

[24] K. O. Mikaelian, Phys. Rev. Lett. **80**, 508 (1998).

[25] P. Ramaprabhu and G. Dimonte, Phys. Rev. E **71**, 036314 (2005).

[26] G. Dimonte, P. Ramaprabhu, D. L. Youngs, M. J. Andrews, and R. Rosner, Phys. Plasmas **12**, 056301 (2005).

[27] B. J. Daly, Phys. Fluids **10**, 297 (1967).

[28] G. Dimonte, Phys. Rev. E **69**, 056305 (2004).

[29] C. L. Gardner, J. Glimm, O. McBryan, R. Menikoff, D. H. Sharp, and Q. Zhang, Phys. Fluids **31**, 447 (1988).

[30] K. I. Read, Physica D **12**, 45 (1984).

[31] D. L. Youngs, Physica D **12**, 32 (1984).

[32] D. L. Youngs, Physica Scripta **92** (2017).

[33] Y. A. Kucherenko, L. I. Shibarshov, S. I. Balabin, and A. P. Pylaev, in *Proceedings of the Third International Workshop on Physics Compressible Turbulent Mixing*, edited by R. Dautray (Commissariat Energie Atomique, Cesta, France, 1991), p. 427.

[34] B. Thornber, D. Drikakis, D. L. Youngs, and R. J. R. Williams, J. Fluid Mech. **654**, 99 (2010).

[35] H. Lim, J. Iwerks, J. Glimm, and D. H. Sharp, Proc. Natl. Acad. Sci. USA **107**, 12786 (2010).

[36] E. George, J. Glimm, X. L. Li, A. Marchese, and Z. L. Xu, Proc. Natl. Acad. Sci. USA **99**, 2587 (2002).

[37] E. George and J. Glimm, Phys. Fluids **17**, 054101 (2005).

[38] D. L. Youngs, Philos. Trans. R. Soc. A **371**, 20120173 (2013).

[39] O. Poujade, Phys. Rev. Lett. **97**, 185002 (2006).

[40] J. R.Ristorcelli and T. T. Clark, J. Fluid Mech. **507**, 213 (2004).

[41] S. W. Haan, Phys. Rev. A **39**, 5812 (1989).

[42] S. W. Haan, Phys. Fluids B **3**, 2349 (1991).

[43] Y.-s. Zhang, L. Li, Z.-w. He, and B.-l. Tian, arXiv:1706.07130 (2017).

[44] D. H. Sharp, Physica D **12**, 3 (1984).

[45] J. Glimm and D. H. Sharp, Phys. Rev. Lett. **64**, 2137 (1990).

[46] J. Glimm, X. L. Li, R. Menikoff, D. H. Sharp, and Q. Zhang, Phys. Fluids A **2**, 2046 (1990).

[47] J. Glimm, D. Saltz, and D. H. Sharp, Phys. Lett. A **222**, 171 (1996).

[48] J. Glimm, Q. Zhang, and D. H. Sharp, Phys. Fluids A **3**, 1333 (1991).

[49] Y. P. Chen, Y. F. Deng, J. Glimm, G. Li, Q. Zhang, and D. H. Sharp, Phys. Fluids A **5**, 2929 (1993).

[50] D. Layzer, Astrophys. J. **122**, 1 (1955).

[51] U. Alon, D. Shvarts, and D. Mukamel, Phys. Rev. E **48**, 1008 (1993).

[52] U. Alon, J. Hecht, D. Mukamel, and D. Shvarts, Phys. Rev. Lett. **72**, 2867 (1994).

[53] J. Hecht, U. Alon, and D. Shvarts, Phys. Fluids **6**, 4019 (1994).

[54] D. Oron, L. Arazi, D. Kartoon, A. Rikanati, U. Alon, and D. Shvarts, Phys. Plasmas **8**, 2883 (2001).

[55] Q. Zhang, Phys. Lett. A **151**, 18 (1990).

[56] J. Glimm and X. L. Li, Phys. Fluids **31**, 2077 (1988).

[57] R. Collins, J. Fluid Mech. **28**, 97 (1967).

[58] R. M. Davies and G. Taylor, Proc. R. Soc. London A **200**, 375 (1950).

[59] D. J. Lewis, Proc. Roy. Soc. London A **202**, 81 (1950).

[60] P. Moin and K. Mahesh, Annu. Rev. Fluid Mech. **30**, 539 (1998).

[61] S. J. Reckinger, J. Reckingera, and O. V. Vasilyev, J. Comput. Phys. **313**, 181 (2016).

[62] G.-S. Jiang and C.-W. Shu, J. Comput. Phys. **126**, 202 (1996).

[63] O. Sadot, V. A. Smalyuk, J. A. Delettrez, D. D.Meyerhofer, T. Sangster, R. Betti, V. N. Goncharov, and D. Shvarts, Phys. Rev. Lett **95**, 265001 (2005).

[64] J. C. V. Hansom, P. A. Rosen, T. J. Goldack, K. Oades, P. Fieldhouse, N. Cowperthwaite, D. L. Youngs, N. Mawhinney, and A. J. Baxter, Laser Part. Beams **8**, 51 (1990).

[65] R. Collins, J. Fluid Mech. **22**, 763 (1965).